

# Parallel *in Vivo* and *in Vitro* Selection Using Phage Display Identifies Protease-dependent Tumor-targeting Peptides<sup>\*§</sup>

Received for publication, April 26, 2010 Published, JBC Papers in Press, May 11, 2010, DOI 10.1074/jbc.M110.138297

Mike Whitney<sup>†</sup>, Jessica L. Crisp<sup>§</sup>, Emilia S. Olson<sup>‡¶</sup>, Todd A. Aguilera<sup>‡¶</sup>, Larry A. Gross<sup>‡||</sup>, Lesley G. Ellies<sup>\*\*</sup>, and Roger Y. Tsien<sup>‡§||1</sup>

From the Departments of <sup>‡</sup>Pharmacology, <sup>§</sup>Chemistry and Biochemistry, and <sup>\*\*</sup>Pathology, the <sup>||</sup>Howard Hughes Medical Institute, and the <sup>¶</sup>Medical Scientist Training Program, University of California at San Diego, La Jolla, California 92093

We recently developed activatable cell-penetrating peptides (ACPPs) that target contrast agents to *in vivo* sites of matrix metalloproteinase activity, such as tumors. Here we use parallel *in vivo* and *in vitro* selection with phage display to identify novel tumor-homing ACPPs with no bias for primary sequence or target protease. Specifically, phage displaying a library of ACPPs were either injected into tumor-bearing mice, followed by isolation of cleaved phage from dissected tumor, or isolated based on selective cleavage by extracts of tumor *versus* normal tissue. Selected sequences were synthesized as fluorescently labeled peptides, and tumor-specific cleavage was confirmed by digestion with tissue extracts. The most efficiently cleaved peptide contained the substrate sequence RLQLKL and labeled tumors and metastases from several cancer models with up to 5-fold contrast. This uniquely identified ACPP was not cleaved by matrix metalloproteinases or various coagulation factors but was efficiently cleaved by plasmin and elastases, both of which have been shown to be aberrantly overexpressed in tumors. The identification of an ACPP that targets tumor expressed proteases without rational design highlights the value of unbiased selection schemes for the development of potential therapeutic agents.

Molecular targeting of contrast and therapeutic agents to tumors is a fundamental goal of cancer research and treatment. Targeting based on tumor-specific molecules has largely relied on binding of antibodies, peptides, or vitamins to antigens or receptors expressed at high levels on tumor cells or their associated vasculature. The drawback to such mechanisms is that they rely on stoichiometric binding that lacks amplification, so either the target must be very highly expressed, or the readout must be extremely sensitive. Activatable cell-penetrating peptides (ACPPs)<sup>2</sup> are a new strategy in which enzymatic amplification drives *in vivo* accumu-

lation of peptide-conjugated cargo within tissues containing active extracellular proteases (1–6). An ACPP consists of three domains: a polycationic cell-penetrating peptide (7–9), a cleavable linker, and a polyanionic inhibitory domain. Before cleavage of the linker, the polyanion pairs with the polycation and prevents cell adhesion and internalization; after cleavage, the polyanion dissociates, unleashing the cell-penetrating peptide to adhere immediately to adjacent cells, followed by cellular internalization. The first ACPPs were designed to be activated by matrix metalloproteinases (MMPs), which are frequently up-regulated in tumors and play a crucial role in extracellular matrix degradation, tissue invasion, and metastasis (10–15). Although an MMP-activated ACPP has been shown to effectively target tumors *in vivo*, this rational design of an ACPP is limited by the availability of known protease substrates and the tissue specific expression of the target protease. For instance, there is currently no known peptide substrate that is perfectly selective for MMPs, and no MMP is exclusively expressed in tumors. Therefore, to improve the applicability of ACPPs, it is important to explore other classes of proteases and substrates with methods that might provide greater specificity and flexibility than *a priori* design.

Previously, phage display technology has been used extensively *in vitro* to identify peptides, proteins, and antibodies based on specific binding or catalytic activity (16–18). In addition, phage display has been used *in vivo* to identify linear or circularized peptides that stoichiometrically bind and accumulate in tumors, synovium, and vascular tissues (19, 20). In this report, we have used phage display to identify peptides that accumulate within tumors *in vivo* as a result of proteolytic modification. This method identifies novel protease substrates that are cleaved within tumors without bias for class of protease or specific substrate sequence. To examine the efficacy of this approach, we performed parallel *in vivo* and *in vitro* selections with phage displaying a library of unique ACPPs. For *in vivo* selection, phage were injected into tumor-bearing mice followed by isolation of cleaved phage from homogenized tumors. For *in vitro* selection, phage were sequentially exposed to normal *versus* tumor tissue extract, followed by isolation of uncleaved or cleaved phage, respectively. Phage selected ACPPs were resynthesized as fluorescently labeled peptides, injected into tumor-bearing mice, and shown to accumulate

\* This work was supported, in whole or in part, by National Institutes of Health, NCI, Grant CA118182 (to L. E.) and DOD grant W81XWH-05-1-0183 (to R. Y. T.).

§ Author's Choice—Final version full access.

¶ The on-line version of this article (available at <http://www.jbc.org>) contains supplemental Figs. 1–6.

<sup>1</sup> To whom correspondence should be addressed: 9500 Gilman Dr., La Jolla, CA 92093. Fax: 619-534-5270; E-mail: rtsien@ucsd.edu.

<sup>2</sup> The abbreviations used are: ACPP, activatable cell-penetrating peptide; MMP, matrix metalloproteinase; SUV, standardized uptake value; Fmoc, N-(9-fluorenyl)methoxycarbonyl; ahx, 6-aminohexyanoyl; TPEN, N,N,N',N'-tetrakis (2-pyridylmethyl) ethylenediamine; NTA, nitrilotriacetic acid; PBS, phosphate-buffered saline; PyMT, polyomavirus middle T antigen; HPLC, high pressure liquid chromatography; Tricine, N-[2-hydroxy-1,1-bis(hy-

droxymethyl)ethyl]glycine; GFP, green fluorescent protein; Mal, maleimide; DTPA, diethylene triamine pentaacetic acid.

within primary and metastatic tumors in a protease-dependent manner.

## EXPERIMENTAL PROCEDURES

**Phage Library Preparation and Selection**—A phage library was generated by PCR, using 5'-primer ggccaagagctccatcatcatcatcatcatctc, 3'-primer ggccagactagtcgcgtcgccgtcg, and oligonucleotide template ccatcatcatcatcatctcgaggaggaggaggaggaggaggaggagggnknnknnknnknnkcgcgacggcgacggcgacggcgacggcgactag, where n denotes any nucleotide and k indicates a mixture of g and t. PCR was performed for 25 cycles with 52 °C annealing and standard reaction conditions. PCR products were digested with restriction enzymes SpeI and SacI for directional cloning into pComb M13 phage expression vector (17). The phage library contained  $5 \times 10^6$  primary transformants, which were converted to infectious phage using helper phage superinfection. Phage libraries were then titrated by infection of XL1blu cells and plated on ampicillin plates. For *in vitro* selections,  $10^9$  phage were incubated for 3 h at 37 °C with mixed liver/kidney tissue extracts equivalent to 2% (2 mg of each tissue per 100 µl). Ni<sup>2+</sup>-NTA-agarose (Qiagen) was added and incubated for 15 min, followed by three washes with PBS. The Ni<sup>2+</sup>-NTA-agarose coupled to the uncleaved phage was then exposed to 2% tumor tissue extract at 37 °C for 3 h. Unbound cleaved phage were eluted from the Ni<sup>2+</sup>-NTA with PBS and plated on XL1blue *E. coli* to recover phage. For *in vivo* selections,  $10^9$  phage in 100 µl of PBS were injected into the tail veins of 10–13-week-old transgenic mice that had 5–15-mm mammary tumors due to expression of PyMT driven by the long terminal repeat of mouse mammary tumor virus. Tumors were excised and homogenized in PBS in the presence of protease inhibitor containing 100 µM 4-(2-aminoethyl)-benzenesulfonyl fluoride-HCl, 80 nM aprotinin, 5 µM bestatin, 1.5 µM E-64, 2 µM leupeptin hemisulfate, and 1 µM pepstatin A (EMD Biosciences mixture III). Uncleaved phage were removed by absorption with Ni<sup>2+</sup>-NTA-agarose, and cleaved phage from the supernatant were reamplified and reinjected into different PyMT tumor-bearing mice.

**Peptide Synthesis and Fluorophore Labeling**—Peptides were either obtained from the W. M. Keck Facility Small Scale Core (Yale University, New Haven, CT) or synthesized in our laboratory on a Perceptive Biosystems Pioneer automatic peptide synthesizer using standard protocols for Fmoc solid-phase synthesis. All peptides were of the general format N terminus-(D-glutamyl)<sub>9</sub>-(6-aminohexanoyl)-(6-amino acid cleavage site)-(D-argininyl)<sub>9</sub>-(either Cy5-D-cysteinate or ε-(fluorescein-5(6)-carbonyl)-L-lysineamide) (see *supplemental Fig. 1* for complete details). Carboxyfluorescein-labeled peptides were generated by Fmoc synthesis with Lys-5(6)-carboxyfluorescein and were acetylated at the N terminus. Albumin-reactive peptide, Mal-e<sub>9</sub>-ahx-RLQLK(Ac)L-r<sub>9</sub>-c(Cy5)-NH<sub>2</sub>, was generated by reacting 3-maleimidopropionic acid pentafluorophenyl ester (Molecular Biosciences) with the free N terminus of Cy5-labeled peptide (see *supplemental Fig. 1* for detailed structures of all peptides). The negative control maleimide (Mal) peptide had -NH(CH<sub>2</sub>CH<sub>2</sub>O)<sub>2</sub>CH<sub>2</sub>CO-, an uncleavable (mpeg) linker (4), in place of the 6-aminohexanoyl and sub-

strate sequence. All Cy5-labeled peptides were purified to greater than 95% purity using C-18 reverse phase HPLC with a 20–50% acetonitrile gradient in 0.1% TFA and the mass was confirmed by mass spectrometry.

**In Vitro Peptide Cleavage**—Tissue extracts were generated by dissecting fresh tissue and gently homogenizing in PBS, while on ice, to minimize the release of intracellular proteases. Homogenates were then microcentrifuged at 14,000 × g for 1 min, and supernatants were recovered and used for *in vitro* testing. All cystic fluids were aspirated with a 28-gauge syringe from surgically exposed mammary tumors of PyMT mice containing fluid filled nodules. *In vitro* cleavages were done with 5 µM peptide in 20 µl of PBS containing 1 µM ZnCl<sub>2</sub> plus 2 µl of 20% tissue extract (20 mg of tissue homogenate per 100 µl) or 2 µl of undiluted cystic fluid, followed by incubation at 37 °C. Aliquots were removed at time intervals from 20 min to 18 h with data being shown for the 2-h time point. For cleavage with purified enzymes, a 50 nM concentration of each enzyme was incubated with 5 µM peptide in the manufacturer's recommended buffer for 4 h. Enzymes and inhibitors were obtained from commercial sources in their active form (a complete table of enzymes and inhibitors is shown in *supplemental Fig. 2*). Tricine sample buffer was added, and treated peptides were boiled for 1 min prior to electrophoresis on 10–20% Tricine acrylamide gels (Invitrogen). Gels were quantitatively imaged on a UVP Biospectrum AC imaging system with external Biolite light source with excitation at 628 ± 20 nm and emission at >700 nm. Quantitation of enzyme cleavage was done using UVP Biospectrum software.

For mass spectrometry determination, each peptide was purified from homogenized cell extract by two steps of reverse phase HPLC. A 30-µl sample of 5 µM ACPP digested with tissue extract for 2 h was diluted to 2.5 ml with solvent A, which contained 2% acetonitrile and 0.14% trifluoroacetic acid. Samples were immediately injected into a Dionex BioLC HPLC system. The autosampler (Gilson model 231) had a 2-ml sample loop, so two 1-ml injections were used for each HPLC chromatogram. The column was a protein C4 from Vydac with a 4.6-mm inner diameter and 25-cm length. The column temperature was 35 °C, and the flow rate was 0.8 ml/min. After an 11-min delay (12% solvent B) for the injections, the gradient was from 12 to 56% solvent B (90% acetonitrile, 0.08% trifluoroacetic acid) in 11 min, followed by a 3-min step of 80% B. The peak eluted at 20 min. Detection was by fluorescence (Dionex RF2000 fluorescence detector, excitation at 640 nm, and emission at 680 nm), and the peak was collected with a Gilson FC203 fraction collector.

For the second step of reverse phase HPLC, the fraction was reconcentrated to 200 µl by centrifuge evaporation (Savant SpeedVac) and then diluted to 600 µl with solvent A again. A Michrom Magic HPLC system was used for liquid chromatography-mass spectrometry, and the column output was detected by a Jasco 920 fluorescence detector and an LTQ Orbitrap XL mass spectrometer. A Michrom sample loop microtrap was used to preconcentrate the entire 600-µl sample for injection. The column was a 1-mm inner dia-

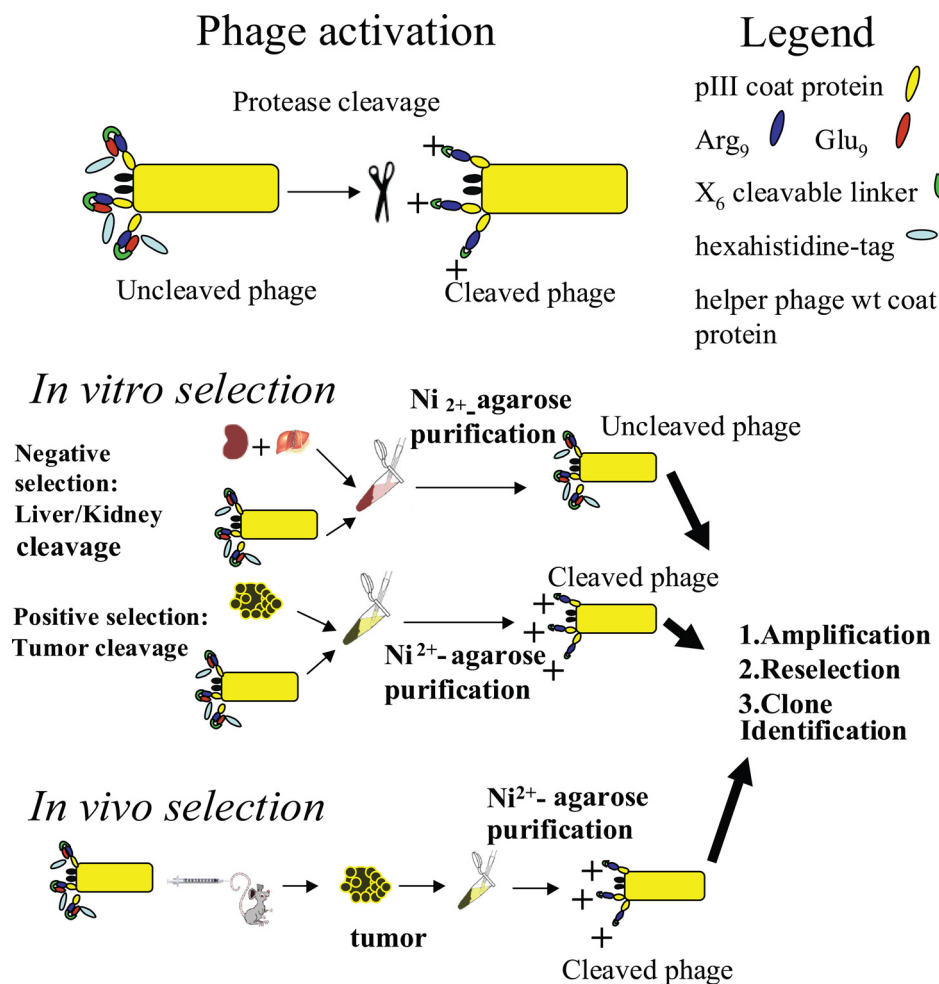


**FIGURE 1.** Parallel *in vivo* and *in vitro* selection with phage display identifies cleavage sequences for protease-dependent tumor targeting. *In vitro*, an M13 phage was generated with a diverse population of ACPPs ( $5 \times 10^6$ ) presented on the surface of the phage. Selection was initiated with  $10^9$  phage, as determined by the number of colony-forming units after superinfection with helper phage and plating on  $100 \mu\text{g}/\text{ml}$  ampicillin plates. All secondary *in vitro* selection was initiated by incubating  $10^9$  with 2% liver/kidney tissue extracts at  $37^\circ\text{C}$  for 3 h. Uncleaved phage selected for resistance to liver/kidney cleavage and therefore less likely to be efficiently cleaved in that tissue were then purified by presence of their hexahistidine tag and exposed to tumor tissue extract for 3 h. Cleaved phage in which the hexahistidine tags were removed by protease cleavage were then collected and reamplified prior to additional selection cycles. Because each phage may have more than one ACPP and associated hexahistidine tag, every ACPP must be cleaved to provide enrichment after purification. Representative phage were sequenced after each round of selection. *In vivo*, phage ( $10^9$  in  $100 \mu\text{l}$  of PBS) were injected into PyMT tumor-bearing mice. After 5 h, mice were sacrificed, and tumors were removed and homogenized to recover phage within the tumor tissue. Phage that had lost their hexahistidine tags due to cleavage within the tumor cells were purified away from uncleaved phage that might be contained in circulating blood at the time of collection. Selected phage were reamplified and iteratively selected in another tumor-bearing mouse, with at least  $10^8$  phage being used for each additional round of selection.

ter, 15-cm Michrom C18AQ, and the fluorescence detector settings were similar to those in the first step. The solvents, column temperature, and gradient were also similar, and the flow rate was  $80 \mu\text{l}/\text{min}$ . The MS was set for  $\sim 0.5$ -s scans with the high resolution Orbitrap from 400 to 2000  $m/z$ . The entire column output went into the mass spectrometer without splitting, using the electrospray interface.

**In Vivo Testing of Peptides**—For each tumor model, Cy5-labeled peptide was injected intravenously via the tail vein. Mice were imaged at time intervals up to 6 h using a Maestro imager (CRI Inc.) with excitation at  $640 \pm 24 \text{ nm}$ , emission at  $>700 \text{ nm}$ . For *in vivo* testing, we used either PyMT mice with spontaneous progressive mammary tumors or nude mice

with 5–7-mm MDA-MB-435 clone M4A4 (gift of D. Tarin, UCSD) xenograft tumors generated by subcutaneous injection of  $10^6$  tumor cells into the mammary fat pads (mice 5–8 weeks of age; Charles Rivers Laboratories). Animals were anesthetized with a 1:1 mixture of 80 mg/kg ketamine and 5 mg/kg midazolam, weighed, and injected with  $100 \mu\text{l}$  of  $100 \mu\text{M}$  free peptides or  $100 \mu\text{l}$  of  $30 \mu\text{M}$  albumin-reactive peptide. After imaging, the animals were euthanized with isoflurane, and tissues were harvested and weighed for standardized uptake values (SUVs). To measure SUVs, 30 mg of each tissue was added to  $100 \mu\text{l}$  of Tris buffer (pH 7.6) with 1% SDS. The tissue was homogenized, heated to  $85^\circ\text{C}$  for 10 min, microwaved for 10 s, centrifuged at  $20,500 \times g$  for 15 min, and imaged on the Maestro imager. Four sets of tissue-specific standards (tumor, liver, kidney, and muscle from non-injected animals, added to known amounts of ACPP and processed as above) were used to calibrate fluorescence intensity in terms of peptide concentration. Tissue-specific standards were necessary because different tissues vary in their ability to quench or conceal Cy5 fluorescence. From this calibration, the quantity of peptide in 30 mg of tissue for each organ was calculated. SUVs were calculated as the molality of peptide in the tissue divided by the total injected dose as mol/kg of body weight. In previous experiments with the MMP-cleavable ACPP, SUVs determined using this method were

similar to SUVs determined using technetium chelates (1, 4–6, 21). Means are given  $\pm$  S.D.; statistical significance of differences was determined by two-tailed *t* tests.

To generate mice with lung metastases,  $5 \times 10^5$  4T1 tumor cells (ATCC) were injected into the tail veins of BALB/c mice 8 days prior to injection with imaging agent. Lungs were removed and imaged either 6 or 48 h postinjection, depending on the peptide construct. Average fluorescent intensity was determined for metastatic lung nodules and compared with adjacent non-malignant tissue or lungs from a tumor-bearing animal that had no lung metastases. We analyzed nine selected regions of 80–200 pixels of each type of tissue, and all tissues were imaged using identical parameters.

## RESULTS

In order to generate a phage library displaying ACPPs, amino acid sequences of the format Met-His<sub>6</sub>-E<sub>9</sub>-X<sub>6</sub>-R<sub>9</sub> (where X<sub>6</sub> represents 6 randomized amino acids) were fused to the N terminus (0–4 copies per phage) of a truncated form of the M13 phage gIII coat protein (17, 22). This library contained  $5 \times 10^6$  putative protease cleavage sites as determined by primary colony-forming units after helper phage infection and dispersal on plates containing antibiotics. This represents about 8% of the potential diversity of  $6.4 \times 10^7$  for X<sub>6</sub>. The X<sub>6</sub> region of the library was generated using NNK(G/T) degenerate oligonucleotides. A hexahistidine motif was added at the N terminus to allow separation by immobilized metal affinity chromatography of unmodified phage from phage whose peptides had been cleaved releasing the hexahistidine tag.

*In vivo* selections were performed by injecting a library of phage displaying recombinant ACPPs intravenously into PyMT mice (Fig. 1). This transgenic breast cancer model produces spontaneous heterogeneous tumors, which can be cystic and will progress to metastasis in older animals (23–25). Six hours after injection, animals were sacrificed, and their tumors were dissected out and homogenized in the presence of protease inhibitors to prevent secondary cleavage of contained phage. Uncleaved phage in the tumor vasculature or nonspecifically localized to tumor at the time of dissection were removed by absorption with Ni<sup>2+</sup>-NTA-conjugated agarose. This purification step was necessary because, as previously reported, phage particles can be retained for long periods in tissues even in the absence of any selection (26). Purified phage that had been cleaved within the mouse were reamplified and injected into different PyMT tumor-bearing mice. This selection was continued for seven iterative cycles with 10–15 individual phage clones being sampled by DNA isolation and sequencing after each round of selection. Five sequences, RLQLKL, RTRYED, RIPLEM, QFDEPR, and TSAVRT, were each isolated multiple times during the *in vivo* selection (Table 1).

For *in vitro* selection, the ACPP phage library was pre-exposed to extracts of liver and kidney, tissues that typically have high nonspecific uptake of drugs and imaging agent, to allow cleavage by proteases contained within these extracts. Ni<sup>2+</sup>-agarose was then used to isolate uncleaved phage that had retained their hexahistidine tags. These preselected phage were then exposed to PyMT tumor extracts and selected for peptide cleavage and loss of their hexahistidine tags. Isolated phage were reamplified and subjected to six additional rounds of both negative (no liver/kidney cleavage) and positive (tumor cleavage) selection, with representative phage being isolated and sequenced after each round. This *in vitro* selection identified five sequences isolated in the *in vivo* selection scheme as well 15 additional sequences (Table 1). Only one sequence, RLQLKL, was identified in duplicate in both the *in vivo* and *in vitro* selection schemes.

To test if isolated peptides corresponding to the phage-selected sequence could be proteolytically cleaved by tumor tissue extracts, 14 of the 21 selected phage sequences were syn-

**TABLE 1**

Phage sequences identified by *in vivo* or *in vitro* selection and cleavage of derived peptides by PyMT tumor tissue extracts

All phage sequences that were identified in at least duplicate from either the *in vivo* or *in vitro* selection are listed. No duplicate phage were identified in either screen prior to the third round of selection. Crude peptides of the format acetyl-e<sub>9</sub>-ahx-X<sub>6</sub>-r<sub>9</sub>-(L-lysine 5(6)-carboxyfluorescein) were synthesized for all phage sequences that were identified three or more times independently. Peptides with internal cysteine residues were excluded because dimerization in protease digest buffer complicated analysis. The percentage of cleavage of crude peptides was determined by digesting 5 μM synthetic peptides with 2% tumor tissue extracts (1 mg of gently homogenized tissue in 50 μl of PBS with 1 mM ZnCl<sub>2</sub>). Quantitation of peptide cleavage was done using gel electrophoresis after a 16-h digestion at 37 °C. The percentage of cleaved *versus* uncleaved peptide was determined using UV imaging software. Four peptides with 6-amino acid cleavage sequences RLQLKL, RTRYED, GMMYRS, and RWRTNF were cleaved >90% after the 16-h digest. These four peptides were therefore prioritized for further study, which included resynthesis and labeling with a longer wavelength Cy5 fluorophore to facilitate *in vivo* testing. NT, not tested.

Cleavage site (X <sub>6</sub> )	<i>In vivo</i> number isolated	<i>In vitro</i> number isolated	Cleavage of e <sub>9</sub> -X <sub>6</sub> -r <sub>9</sub> peptide by tumor extract
RLQLKL	2	11	>90
RTRYED	3		>90
RIPLEM	3		<10
QFDEPR	3		<10
TSAVRT	2		NT
GLWQGP		7	~20
QCTGRF	1	5	NT
LPGMMG		5	~20
DVGTTE		5	No cleavage
TDLGAM		5	No cleavage
GMMYRS		4	>90
DSNAES		4	No cleavage
ITDMAA	1	3	~20
RWRTNF		4	>90
WRPCES	1	2	NT
WRNTIA		3	~50
IDKQLE		3	<5
FMEIET		3	<5
HEVVAG		2	NT
GGHTRQ		2	NT
INGKVT		2	NT

thesized as peptides in the format acetyl-e<sub>9</sub>-(ahx)-X<sub>6</sub>-r<sub>9</sub>-5(6)-carboxyfluorescein-labeled L-lysinamide using solid-phase synthesis (for complete structures, see supplemental Fig. 1). The (ahx) denotes 6-aminoheptanoyl, a flexible linker that is included in ACPPs to give the cleavable X<sub>6</sub> domain the ability to adopt a more extended conformation within the protease cleavage domain. The polyglutamate and polyarginine segments consisted entirely of D-amino acids (denoted by lowercase letters) in order to maximize their resistance to proteolysis *in vivo*. Four peptides, containing X<sub>6</sub> = RLQLKL, RTRYED, GMMYRS, and RWRTNF, were cleaved >80% by tumor tissue extract after 16-h digestions at 37 °C (Table 1).

These top four peptides were resynthesized in the format H<sub>2</sub>N-e<sub>9</sub>-(ahx)-X<sub>6</sub>-r<sub>9</sub>-(Cy5-labeled D-cysteinamide), followed by purification to greater than 95% for *in vitro* and *in vivo* testing. Each of these peptides was tested for differential cleavage by tumor *versus* mixed liver/kidney tissue extracts after a 2-h digestion compared with the 16-h digestion shown in Table 1 (Fig. 2A). All four peptides were cleaved >50% by tumor tissue extract, with RLQLKL being the most rapidly cleaved, >90% after 4 h (full time course not shown). Each peptide except for GMMYRS showed increased cleavage by tumor extract relative to mixed liver/kidney extracts. A control peptide with all D-amino acids, X<sub>6</sub> = rlqlkl, was not cleaved by any of the tissue extracts.

## Identification of Protease-dependent Tumor-targeting Peptides

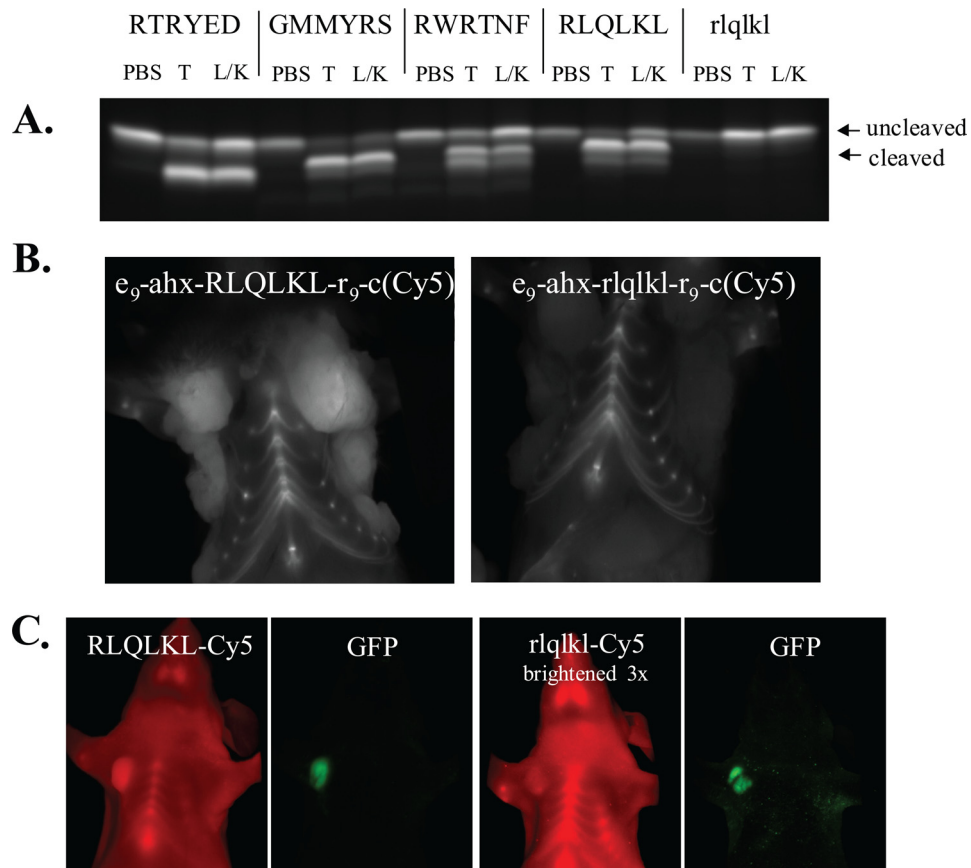


**FIGURE 2.** *A*, *in vitro* characterization of five Cy5-labeled ACPPs containing RTRYED, GMMYRS, RWRTNF, RLQLKL, and rlqlkl at the protease cleavage site. Uppercase and lowercase letters denote L- and D-amino acids, respectively. For each reaction, 5  $\mu$ M ACPP was incubated with either 2% tumor or 2% liver/kidney tissue extracts at 37 °C for 2 h (compared with 16 h; Table 1). Cleavage was detected by electrophoresis on 16% Tricine acrylamide gels. RLQLKL, RTRYED, and RWRTNF ACPPs were more efficiently cleaved by tumor extract *versus* liver/kidney extracts (see ratio of cleaved to uncleaved). Of these, RWRTNF showed the greatest differential cleavage by tumor *versus* liver/kidney extracts. As expected, the all-D-rlqlkl peptide showed no cleavage under any of the tested conditions. *B*, *in vivo* characterization of tumor uptake on mice injected with Cy5-labeled ACPPs. PyMT tumor-bearing mice were imaged 6 h after injection with 100  $\mu$ l of a 100  $\mu$ M concentration of either the protease-cleavable ACPP NH<sub>2</sub>-e<sub>9</sub>-(ahx)-RLQLKL-r<sub>9</sub>-c-(Cy5)-NH<sub>2</sub> (*left*) or the uncleavable all D-amino acid control peptide NH<sub>2</sub>-e<sub>9</sub>-(ahx)-rlqlkl-r<sub>9</sub>-c(Cy5)-NH<sub>2</sub>. Images with skin removed are shown because they highlight the variability of the labeling throughout the tumor. Skin-off images also eliminate artifacts that sometime appear due to incomplete shaving of the animal or nicks that occur during shaving. Skin-on images are shown for comparison in *supplemental Fig. 2*. Tissues were removed post mortem for SUV determination. *C*, nude mice with MDA-MB-435 M4A4 xenografts expressing GFP were injected with either RLQLKL ACPP (*far left*) or control rlqlkl peptide (*middle right*), 100  $\mu$ l of 100  $\mu$ M in each case. The RLQLKL ACPP gave visible contrast in tumors that were confirmed by imaging GFP fluorescence. Mice injected with rlqlkl peptide showed no tumor contrast in the Cy5 channel (*middle right*), although the tumor was clearly visible by GFP (*far right*). All images were taken 6 h after injection, in live animals with skin on, using identical settings on the Maestro imager. Images for rlqlkl peptides were brightened 3-fold to illustrate the lack of contrast for tumor compared with surrounding tissue for the uncleavable control.

In order to compare *in vivo* tumor labeling, these four Cy5-labeled ACPPs were separately injected intravenously into PyMT mice with spontaneous mammary tumors. Six hours postinjection, mice were imaged by fluorescence to show contrast of tumor compared with adjacent normal tissue. The most striking visual contrast for tumor uptake was obtained from mice injected with the RLQLKL ACPP (Fig. 2*B*). Consistent with this high visual contrast, the SUVs in the tumor, defined as the molality of Cy5 in the specific tissue divided by the molality of the injected dose for the total weight of the animal, was the highest for the RLQLKL ACPP at 0.39 ± 0.14 ( $n = 8$ ). This compared with the uncleavable all-D-amino acid peptide, rlqlkl ACPP, which had a SUV of 0.13 ± 0.03

( $n = 3$ ) with  $p = 0.014$ . The decreased tumor accumulation in the mice injected with the uncleavable D-amino acid probe of identical molecular weight and hydrophobicity strongly suggests that tumor uptake is dependent on protease susceptibility rather than nonspecific adhesion or enhanced vascular permeability of tumors. This ratio of 3 between protease-sensitive and relatively insensitive peptides compares with a ratio of 3.6 for our previous ACPP, in which  $X_6$  = PLGLAG and targets matrix metalloproteinases (1). PLGLAG ACPP had SUV values of 0.51 ± 0.05 ( $n = 5$ ) *versus* 0.14 ± 0.06 ( $n = 5$ ),  $p < 0.01$ , for its D-amino acid control. As with all free peptide ACPPs, there is labeling of cartilaginous portions of the anterior ribcage (4, 5). One advantage of RLQLKL ACPP *versus* PLGLAG ACPP is that skin uptake was significantly less, improving contrast during noninvasive visualization in live animals (see *supplemental Fig. 3* for images).

To explore whether RLQLKL ACPP could be used as a contrast agent for tumor models other than the PyMT mice, Cy5-labeled RLQLKL ACPP and its all-D-amino acid control were tested in mice bearing MDA-MB-435 M4A4 human xenografts. This tumor model (also known as M14 melanoma (27)) was stably transfected with GFP for unambiguous identification of xenograft *versus* host tissue. Tumors of mice injected with the RLQLKL ACPP showed far red (Cy5) fluorescence, which co-localized with the GFP fluorescence (Fig. 2*C*). Mice injected with the uncleavable D-amino acid (rlqlkl) control showed much less Cy5 fluorescence within the tumors, which were still clearly visible by GFP fluorescence. Tumor SUVs 6 h after injection were also significantly higher for the RLQLKL ACPP 0.70 ± 0.27 ( $n = 6$ ) compared with 0.34 ± 0.16 ( $n = 6$ ) for rlqlkl control peptide ( $p = 0.022$ ).

To characterize the protease activity responsible for tumor uptake, the effect of various protease inhibitors on tissue extract mediated cleavage of RLQLKL ACPP was tested. Unfortunately, cleavage of RLQLKL ACPP by crude tissue extracts is quite resistant to inhibition by protease inhibitors, which may be due to high protease activity in tissue extracts or the multiplicity of proteases released upon tissue disruption. We there-

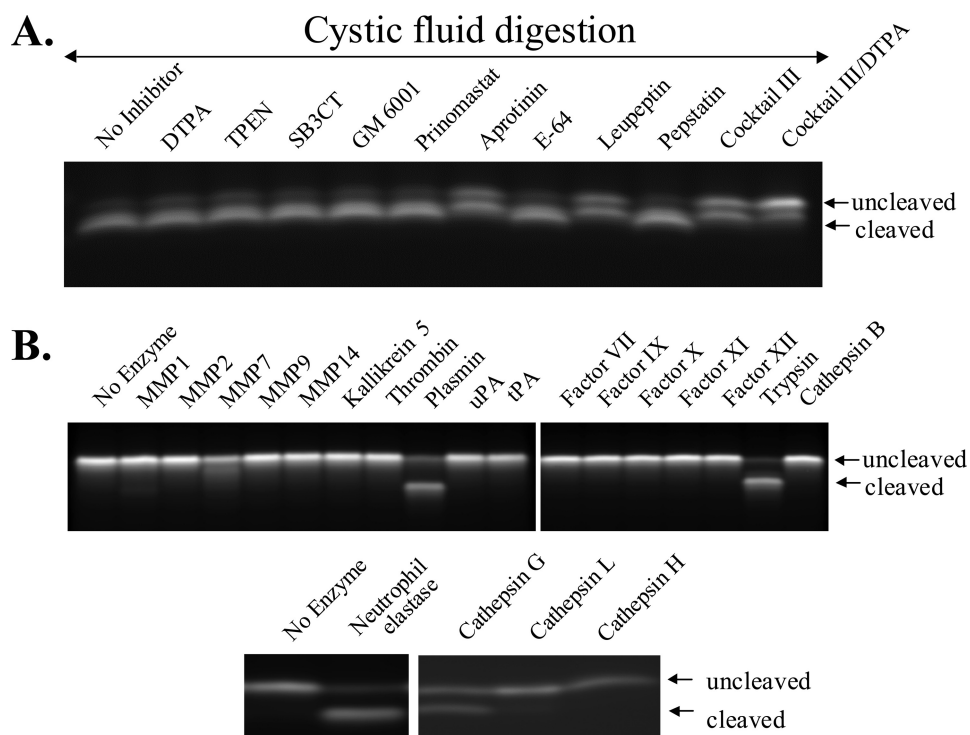


**FIGURE 3. Effects of enzymes and inhibitors on cleavage of the RLQLKL ACPP *in vitro*.** *A*, cleavage of 5  $\mu$ M Cy5-labeled RLQLKL ACPP for 2 h with 2% cystic fluid obtained from PyMT tumors, in the absence of inhibitor or with 5 mM Ca-DTPA, 50  $\mu$ M TPEN, 18  $\mu$ M SB3CT (43), 50 nM GM6001 (also tested at 1  $\mu$ M and no inhibition; data not shown), 0.26  $\mu$ M prinomastat, 150 nM aprotinin, 10  $\mu$ M E-64, 100  $\mu$ M leupeptin, 1  $\mu$ M pepstatin A, Calbiochem mixture III (diluted 1:1000), mixture III + DTPA. All inhibitors were used at the manufacturers' recommended concentrations, which should inhibit  $\geq 95\%$  of the target enzymes' activity. *B*, cleavage of RLQLKL ACPP for 2 h with 50 nM MMP-1, MMP-2, MMP-7, MMP-9, MMP-14, kallikrein 5, thrombin, plasmin, urokinase plasminogen activator, tissue plasminogen activator, factor VIIa, factor IXa, factor Xa, factor XIa, factor XIIa, trypsin (cathepsins B, G, L, and H), and neutrophil elastase. The percentage of cleavage measured with UVP software was 93.0  $\pm$  2.9% for trypsin, 79.0  $\pm$  2.8% for neutrophil elastase, 77.9  $\pm$  2.1% for plasmin, 60%  $\pm$  2.3% for cathepsin G, 23.4  $\pm$  2.5% for MMP7, 9.7  $\pm$  1.1% for MMP1, and less than 3% for all other enzymes tested, including hepsin, enterokinase, and prostate-specific antigen (*supplemental Fig. 4*). MMP-8, MMP-13, matriptase, urokinase, and legumain also showed no cleavage (data not shown). Trypsin and trypsin-2 cleavage of various ACPP are also shown in *supplemental Fig. 4*.

fore switched to cystic fluid obtained from fluid-filled nodules of PyMT tumors because this fluid probably contained proteases that had been secreted by adjacent tumor tissue and was less likely than tumor extracts to be contaminated with intracellular proteases. The use of similar tumor cystic fluids (although obtained from pancreatic and not mammary tumors) for cancer protease profiling has been reported elsewhere (28, 29). Cystic fluid cleaved RLQLKL ACPP similarly to tumor tissue extracts, and this cleavage was partially inhibited by two serine protease inhibitors, aprotinin and leupeptin (Fig. 3A). This inhibitor profile supported the involvement of a serine protease in the *in vivo* cleavage and tumor uptake of RLQLKL ACPP.

Cleavage of RLQLKL ACPP was further investigated using a panel of candidate proteases. The serine proteases plasmin, trypsin, and neutrophil elastase were the only enzymes found to efficiently cleave RLQLKL ACPP (Fig. 3B and *supplemental Fig. 4*). Each of these proteases has been reported to be up-regulated in cancers. There was also minimal cleavage of RLQLKL ACPP by cathepsin G, MMP-1, MMP-7, and MMP12, which at times was only visible upon gel overexposure. MMPs are not likely to be responsible for *in vivo* tumor uptake because they exhibit low cleavage rates.

Additionally, cleavage by cystic fluid was unaffected by MMP-specific inhibitors (GM6001, SB3CT, prinomastat) and Zn<sup>2+</sup> chelators (DTPA and TPEN). Plasmin has been reported to be associated with tumor vasculature, and urokinase plasminogen activator is known to be preferentially activated in PyMT tumors (30–32). The plasmin-specific inhibitor serpin F2/ $\alpha_2$ -antiplasmin, however, did not inhibit the protease activity of cystic fluid or tumor extract on RLQLKL ACPP, although it did inhibit plasmin cleavage, as expected (Fig. 4A). This result indicated that plasmin was probably not responsible for tumor extract cleavage or *in vivo* uptake of RLQLKL ACPP. Another candidate protease for *in vivo* cleavage of RLQLKL ACPP, trypsin, is normally produced by the pancreas as a zymogen (trypsinogen) and is later modified into its active form by enterokinase. Trypsin and trypsin-like protease expression has been reported in malignant non-pancreatic cells and has been shown to stimulate cancer cell growth in culture and in nude mice (33–36). However, trypsin cleavability correlated poorly with *in vivo* uptake because trypsin, unlike elastase, efficiently cleaved RTRYED and GMMYRS ACPPs, but these peptides showed little fluorescence contrast in tumors relative to adjacent normal tissue (data not shown). Elastase, a component of breast milk, has been reported to be expressed in breast cancer cell lines and has been implicated as a factor in both the prognosis and progression of breast cancer (37–39). Although this protein is expressed ubiquitously, high circulating levels of its natural inhibitor  $\alpha_1$ -antitrypsin (up to 50  $\mu$ M) prevent its activity in the bloodstream. We found that  $\alpha_1$ -antitrypsin inhibited the protease activity of cystic fluid and was also the only inhibitor tested that significantly inhibited tumor extract-dependent cleavage of RLQLKL ACPP (Fig. 4B, top). This inhibition increased as the concentration of tumor extract was reduced from 2 to 0.25%. Additionally, both the highly related pancreatic form of elastase and leukocyte elastase (ELA-2 from a different source) effectively cleaved RLQLKL ACPP.

To further characterize the proteolytic cleavage and means of tumor uptake of RLQLKL ACPP, mass spectrometry was used to compare the proteolytic cleavage products produced by exposure to liver, kidney, and tumor extracts to those produced after cleavage by plasmin, trypsin, and elastase

## Identification of Protease-dependent Tumor-targeting Peptides

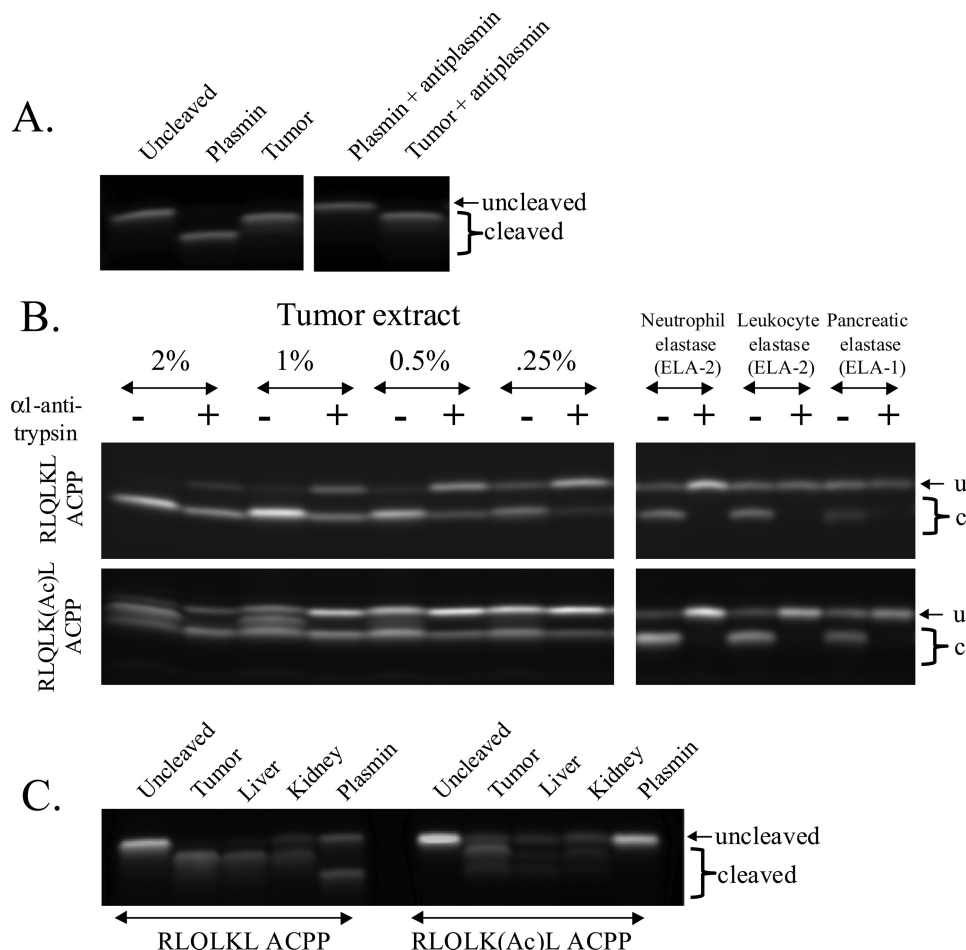


FIGURE 4. A, cleavage of  $5 \mu\text{M}$  Cy5-labeled RLQLKL ACPP by plasmin and tumor extract with and without plasmin-specific inhibitor F2/ $\alpha_2$ -antiplasmin. B, cleavage of  $5 \mu\text{M}$  Cy5-labeled RLQLKL or RLQLK(Ac)L ACPP with varied amounts of tumor extract (2.0 to 0.25%), neutrophil/leukocyte elastase (ELA-2, two sources) or pancreatic elastase (ELA-1) in the presence or absence of  $60 \mu\text{M}$   $\alpha_1$ -antitrypsin. C, comparison of RLQLK(Ac)L ACPP with parent RLQLKL ACPP. For each reaction,  $5 \mu\text{M}$  purified Cy5-labeled peptide was incubated with either 2% tumor, 2% liver, or 2% kidney tissue extracts or  $50 \text{ nM}$  plasmin at  $37^\circ\text{C}$  for 2 h. Cleavage was detected by electrophoresis on 16% Tricine acrylamide gels.

(supplemental Fig. 5). The cleavage products produced by tissue extract cleavage are inherently variable, depending on time of digest, batch, and concentration of tissue extract. However, it was determined that cleavage of RLQLKL ACPP by either kidney or tumor extracts produced in differing ratios three detectable cleavage products, corresponding to (LKL<sub>r,c</sub>-(Cy5), K<sub>r,c</sub>-(Cy5), and L<sub>r,c</sub>-(Cy5)). K<sub>r,c</sub>-(Cy5) was the most abundant cleavage product after treatment with tumor extracts, whereas each of the three cleavage products was represented about equally when cleaved by kidney. In contrast, cleavage by liver produced only one product L<sub>r,c</sub>-(Cy5), which suggests that liver cleavage was due to different endoproteases from kidney and tumor or alternatively that liver was much more efficient at removing leucine and/or lysine from either LKL<sub>r,c</sub>-(Cy5) or K<sub>r,c</sub>-(Cy5). Digestion of RLQLKL ACPP with either plasmin or trypsin produced the single cleavage product L<sub>r,c</sub>-(Cy5), suggesting that these enzymes may be responsible for liver but not tumor cleavage. In contrast, like tumor extract, cleavage by either pancreatic or neutrophil elastase produced as their major product

K<sub>L,r,c</sub>-(Cy5), supporting elastases as a good target enzyme for *in vivo* tumor uptake of RLQLKL ACPP.

To improve tumor-selective cleavage of RLQLKL ACPP, a modified version was generated in which the  $\epsilon$ -amino group of lysine was acetylated. We hypothesized that because lysine is the site of cleavage by liver extracts and the non-target enzymes trypsin and plasmin, acetylation at this residue should increase tumor selectivity by reducing off-target cleavage. Indeed, this new RLQLK(Ac)L ACPP was not cleaved by plasmin, although it was efficiently cleaved by tumor extracts (Fig. 4C). As predicted, cleavage of this acetylated ACPP by liver and kidney tissue extracts was also significantly reduced compared with the parent RLQLKL ACPP, thereby further enhancing selectivity for tumor cleavage. Interestingly, tumor extract cleavage of RLQLK(Ac)L ACPP produced two bands by electrophoresis gel analysis (Fig. 4B, bottom). The generation of one of these bands upon digestion with tumor extract could be efficiently inhibited by the addition of  $\alpha_1$ -antitrypsin, whereas production of a lower molecular weight cleavage product showed little or no inhibition. This further supported elastase as a target enzyme but highlights the presence of at least one additional

protease within tumor extracts that can cleave and potentially enhance tumor uptake of RLQLK(Ac)L ACPP. The presence of neutrophil elastase within PyMT tumor extracts was confirmed by Western blot analysis (supplemental Fig. 6). Mass spectrometry was used to analyze cleavage products produced by tumor extract in the presence and absence of  $\alpha_1$ -antitrypsin, but variability between tumor extract preparations, incomplete inhibition, and heterogeneity of cleavage products prevented the identification of a specific cleavage product that was inhibited by  $\alpha_1$ -antitrypsin. We were, however, able to confirm that as with RLQLKL ACPP, cleavage of RLQLK(Ac)L ACPP by tumor extracts or elastases produced the same major product, K(Ac)L<sub>r,c</sub>-(Cy5) (supplemental Fig. 5).

To test *in vivo* uptake, Cy5-labeled RLQLK(Ac)L ACPP was injected into PyMT tumor-bearing mice. This optimized ACPP was taken up in tumors to levels equal to or slightly greater than the unmodified parent RLQLKL ACPP ( $\text{SUV} = 0.39 \pm 0.14$  ( $n = 8$ ) for RLQLKL and  $0.48 \pm 0.04$  ( $n = 3$ ) for RLQLK(Ac)L,  $p = 0.33$ ), supporting the hypothesis that elastase but not plasmin could be responsible for tumor uptake in the PyMT model

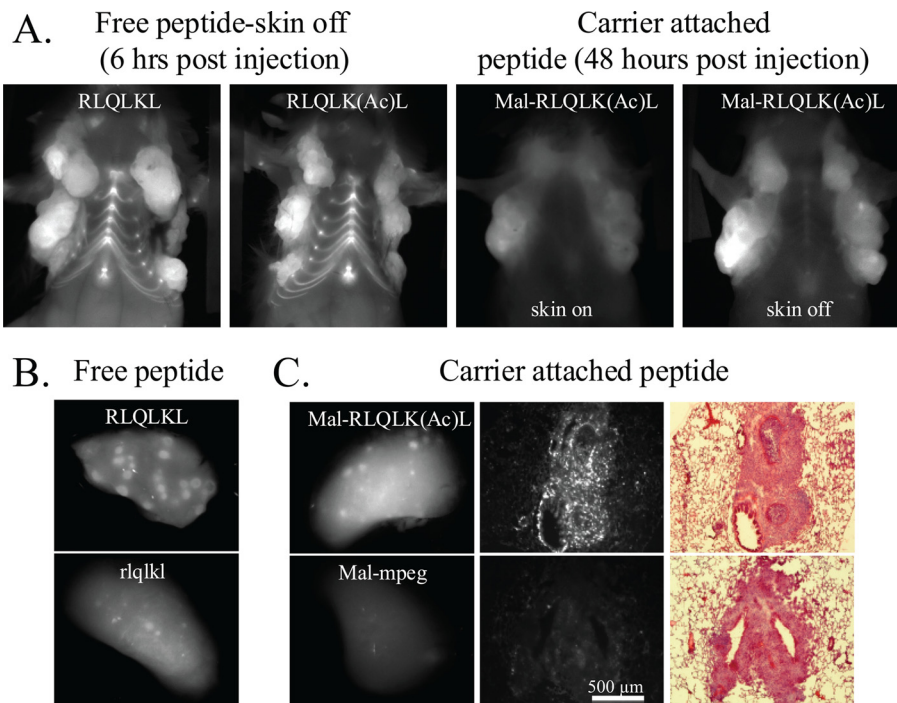


**FIGURE 5.** *A*, *in vivo* characterization of tumor uptake on mice injected with Cy5-labeled RLQLK(Ac)L ACPP and albumin-reactive Mal-e<sub>9</sub>-(ahx)-RLQLK(Ac)L-r<sub>9</sub>-c(Cy5)-NH<sub>2</sub> ACPP compared with parent RLQLKL ACPP. PyMT tumor-bearing mice were imaged 6 h after injection with 10 nmol of either H<sub>2</sub>N-e<sub>9</sub>-(ahx)-RLQLKL-r<sub>9</sub>-c(Cy5)-NH<sub>2</sub> (*left*) or H<sub>2</sub>N-e<sub>9</sub>-(ahx)-RLQLK(Ac)L-r<sub>9</sub>-c(Cy5)-NH<sub>2</sub> PyMT tumor-bearing mouse imaged 48 h after injection with 3 nmol of Mal-e<sub>9</sub>-(ahx)-RLQLK(Ac)L-r<sub>9</sub>-c(Cy5)-NH<sub>2</sub> (*right*) (complete structures diagramed in *supplemental Fig. 1*). Skin-off images are shown for free peptide (*left*), and skin-off/skin-on images are shown for albumin-reactive peptide (*right*). Tissues were removed post mortem for SUV determination. *B*, detection of PyMT lung metastases and seeded lung tumors with various ACPPs. PyMT tumor mice were injected with free peptide RLQLKL ACPP. Lungs were removed and imaged 6 h postinjection. Lung metastases were seen as distinct fluorescent spots compared with adjacent tissue, within the lungs (*top*). Fluorescent spots were verified to be metastasis by hematoxylin/eosin staining (*supplemental Fig. 4*). Lungs from animals injected with uncleavable control rlqlkl show much less distinct fluorescent spots (*bottom*). Metastases were confirmed to be of similar size. *C*, lungs from mice that had been generated by seeding 4T1 tumor cells into lungs 10 days prior to injection of contrast agent. Mice were injected with either Mal-RLQLK(Ac)L ACPP (*top row*) or an uncleavable Mal-mpeg-ACPP (*bottom row*) and imaged. Lungs were then sectioned, and serial sections were either imaged for Cy5 fluorescence or used for hematoxylin/eosin staining. Bright fluorescence in the *top center* was from a single metastatic nodule.

(Fig. 5*A*, *top left*). In addition to improved specificity, acetylation of the RLQLKL ACPP simplifies attachment of dyes or other functional groups to the N-terminal amine of the peptide by blocking cross-reactivity to the lysine within the protease cleavage site.

To increase tumor-specific uptake relative to background tissues, RLQLK(Ac)L ACPP was additionally modified by conjugating a maleimide (Mal) group to the N-terminal amine, thereby generating an albumin-reactive peptide (40, 41). The rapid covalent attachment of this thiol-reactive peptide, Mal-RLQLK(Ac)L ACPP, to a cysteine on serum albumin increases the molecular size of the imaging agent, thereby increasing the blood circulation time while decreasing renal and synovial filtration. The albumin-reactive ACPP was injected into PyMT tumor-bearing mice and imaged 48 h postinjection before and after skin removal. Tumor to non-tumor contrast was 5.1-fold for the Mal-RLQLK(Ac)L ACPP, compared with less than 3-fold for free peptide RLQLK(Ac)L ACPP (Fig. 5*A*). SUVs were  $2.3 \pm 0.6$  ( $n = 3$ ) for the albumin-reactive ACPP compared with  $0.48 \pm 0.04$  ( $n = 3$ ) for free peptide RLQLK(Ac)L ACPP. Background labeling of cartilage and bone was also greatly

decreased, consistent with previously reported data for macromolecule-conjugated ACPPs (5).

In addition to identifying primary tumors, RLQLKL ACPP was used for the detection of lung metastases in PyMT mice. These spontaneous lung metastases (which occur sporadically in older animals) were clearly visible as bright fluorescent spots compared with adjacent normal lung tissue (Fig. 5*B*, *top*). These zones were confirmed as metastases by hematoxylin and eosin staining of paraffin-embedded sections (*supplemental Fig. 6*). Lungs from similar animals without metastases (also from animals with primary tumors) were uniformly dim (*supplemental Fig. 6*) and were 4.2-fold ( $p < 0.01$ ) less bright than metastatic nodules on average. Non-malignant tissue adjacent to metastases appeared brighter than tissue from lungs with no metastases, possibly because some of the fluorescence from metastases scattered into adjacent lung tissue or because some protease-secreting cells, protease, or cleaved peptide spread from the metastasis into the surrounding tissue. For comparison, the rlqlkl control peptide showed much reduced contrast compared with the RLQLKL ACPP (Fig. 5*B*, *bottom*). The small amount of contrast observed for metastasis from mice that had been injected with rlqlkl ACPP may be due

to the differential cell density of lung metastasis *versus* normal lung tissue. Unfortunately, lung metastases were present in only a fraction of PyMT tumor-bearing mice, so data were obtained from only a few animals.

To further study the labeling of metastases by RLQLK(Ac)L ACPP, a new experimental lung metastasis model was generated by injecting 4T1 tumor cells intravenously and allowing them to seed in the lungs. Lungs from mice that had been injected with either Mal-RLQLK(Ac)L ACPP or uncleavable Mal-mpeg-ACPP were removed and imaged. Again, the cleavable probe highlighted fluorescent nodules, which were confirmed by hematoxylin and eosin staining to be metastases (Fig. 5*C*, *top row*). The uncleavable control showed little or no uptake in metastases (Fig. 5*C*, *bottom row*). Lung sections viewed at higher magnification showed that the fluorescence from the albumin-reactive cleavable ACPP was distributed throughout the metastatic nodules and originated from numerous 10–50- $\mu$ m punctae, which could represent labeling of individual or small clusters of cells. These results conclusively demonstrated specific labeling of lung metastases with this newly identified elastase-cleavable ACPP.

## DISCUSSION

Phage display identified the RLQLKL ACPP as a promising new tool that has the ability to detect protease activity in tumors and could be used to direct therapeutic or imaging agents to cancer cells *in vivo*. This selected ACPP was modified using a non-native amino acid, *N*<sup>ε</sup>-acetyl-lysine, to further enhance its enzyme selectivity and specific tumor uptake. Modification of the lysine residue within the protease cleavage site facilitates attachment to a large molecular weight carrier, such as albumin. Further modification of our current best substrate RLQLK(Ac)L ACPP by genetic or synthetic iteration around the RLQLKL cleavage sequence (e.g. holding some residues constant while exhaustively varying the remainder) could provide additional optimization. *In vivo* properties could be further modulated by attachment to other high molecular weight carriers for improved pharmacokinetics or increased valency of the ACPP to enhance tissue specific uptake.

In addition, because this method identifies a specific ACPP cleavage sequence (in this case RLQLKL and the acetylated derivative), traditional biochemical techniques, including inhibitor and enzyme assays, extraction methods, or activity-based protease profiling (42), can be used to identify the target protease(s). We have used these techniques to characterize the cleavage of RLQLKL ACPP and demonstrate cleavage by multiple serine proteases. We then generated an improved, acetylated substrate that was still efficiently cleaved by tumor extracts and elastases but had reduced cleavage by liver and kidney and was not cleaved by plasmin. Based on this and other presented data showing expression of elastase in PyMT tumors and inhibition of protease activity in tumor extracts by  $\alpha_1$ -antitrypsin and prior reports of elastase expression in breast cancers, we postulate that elastases are probably responsible for a major part of tumor uptake of RLQLKL ACPPs in PyMT tumors. Despite this claim, the identification of one specific protease that is responsible for 100% of cleavage and tumor uptake of any specific ACPP may not be possible because cleavage and tumor uptake probably results from a plurality of proteases present in the extracellular matrix of tumors. Additionally complicating the one enzyme-targeted mechanism is that peptide substrates and inhibitors that are exquisitely specific to a single protease remain a biochemical challenge. Interestingly, the identification of a protease substrate that is cleaved by multiple proteases could be expected based on the presented selection strategy that identified phage modified by extracellular enzymes expressed by tumors that probably contained more than one protease. Validation of this possibility for *in vivo* substrate cleavage by a multiplicity of proteases and utilizing this as a tool for synergistic multiprotease tumor targeting would represent a novel mechanism for targeting cancers and other tissues.

To highlight the technical improvements in the novel phage selection strategy presented here, it must be compared with prior *in vivo* phage selections. Previously published *in vivo* phage selection strategies relied almost entirely on tissue-specific binding, whereas the selection scheme presented here represents a novel use of phage display as an unbiased way to identify sites of *in vivo* enzymatic activity, in this case protease

activity within tumors. Our strategy includes selection for covalent modification of the targeting sequence and not simply binding to the target tissue. Exclusive reliance on such tissue binding and localization for selection has the problem that phage particles have been shown to be nonspecifically retained in tissues for  $\geq 24$  h after *in vivo* injection (26). Future selections using our new strategy could become more elaborate by targeting specific intracellular compartments, either by including subcellular fractionation in the recovery step or by selecting for a compartment-specific biochemical modification, such as phosphorylation or biotinylation.

**Acknowledgments**—We thank Evangeline Mose, Holly Weld, Tim Salazar, Rachel Levin, and Perla Arcaira for technical assistance with SUVs and phage injections; Tao Jiang for discussions and training in peptide synthesis; Pfizer for a gift of prinomastat; and B. Ondek, S. Rodems, and Marco Gallio for critical review of and suggestions on the manuscript.

## REFERENCES

1. Jiang, T., Olson, E. S., Nguyen, Q. T., Roy, M., Jennings, P. A., and Tsien, R. Y. (2004) *Proc. Natl. Acad. Sci. U.S.A.* **101**, 17867–17872
2. Goun, E. A., Shinde, R., Dehnert, K. W., Adams-Bond, A., Wender, P. A., Contag, C. H., and Franc, B. L. (2006) *Bioconjug. Chem.* **17**, 787–796
3. Zhang, Y., So, M. K., and Rao, J. H. (2006) *Nano Lett.* **6**, 1988–1992
4. Aguilera, T. A., Olson, E. S., Timmers, M. M., Jiang, T., and Tsien, R. Y. (2009) *Integrative Biology* **1**, 371–381
5. Olson, E. S., Aguilera, T. A., Jiang, T., Ellies, L. G., Nguyen, Q. T., Wong, E. H., Gross, L. A., and Tsien, R. Y. (2009) *Integrative Biology* **1**, 382–393
6. Olson, E. S., Jiang, T., Aguilera, T. A., Nguyen, Q. T., Ellies, L. G., Scadeng, M., and Tsien, R. Y. (2010) *Proc. Natl. Acad. Sci. U.S.A.* **107**, 4311–4316
7. Gammon, S. T., Villalobos, V. M., Prior, J. L., Sharma, V., and Piwnica-Worms, D. (2003) *Bioconjug. Chem.* **14**, 368–376
8. Rothbard, J. B., Kreider, E., VanDeusen, C. L., Wright, L., Wylie, B. L., and Wender, P. A. (2002) *J. Med. Chem.* **45**, 3612–3618
9. Wright, L. R., Rothbard, J. B., and Wender, P. A. (2003) *Curr. Protein Pept. Sci.* **4**, 105–124
10. Bremer, C., Bredow, S., Mahmood, U., Weissleder, R., and Tung, C. H. (2001) *Radiology* **221**, 523–529
11. Bremer, C., Tung, C. H., and Weissleder, R. (2001) *Nat. Med.* **7**, 743–748
12. La Rocca, G., Pucci-Minafra, I., Marrazzo, A., Taormina, P., and Minafra, S. (2004) *Br. J. Cancer* **90**, 1414–1421
13. Ratnikov, B. I., Deryugina, E. I., and Strongin, A. Y. (2002) *Lab. Invest.* **82**, 1583–1590
14. Sounni, N. E., Janssen, M., Foidart, J. M., and Noel, A. (2003) *Matrix Biol.* **22**, 55–61
15. Talvensaari-Mattila, A., Pääkkö, P., and Turpeenniemi-Hujanen, T. (2003) *Br. J. Cancer* **89**, 1270–1275
16. Atwell, S., and Wells, J. A. (1999) *Proc. Natl. Acad. Sci. U.S.A.* **96**, 9497–9502
17. Barbas, C. F., 3rd, Kang, A. S., Lerner, R. A., and Benkovic, S. J. (1991) *Proc. Natl. Acad. Sci. U.S.A.* **88**, 7978–7982
18. Kridel, S. J., Sawai, H., Ratnikov, B. I., Chen, E. I., Li, W., Godzik, A., Strongin, A. Y., and Smith, J. W. (2002) *J. Biol. Chem.* **277**, 23788–23793
19. Laakkonen, P., Akerman, M. E., Biliran, H., Yang, M., Ferrer, F., Karpanen, T., Hoffman, R. M., and Ruoslahti, E. (2004) *Proc. Natl. Acad. Sci. U.S.A.* **101**, 9381–9386
20. Mi, Z., Lu, X., Mai, J. C., Ng, B. G., Wang, G., Lechman, E. R., Watkins, S. C., Rabinowich, H., and Robbins, P. D. (2003) *Mol. Ther.* **8**, 295–305
21. Thie, J. A. (2004) *J. Nucl. Med.* **45**, 1431–1434
22. Sidhu, S. S. (2001) *Biomol. Eng.* **18**, 57–63
23. Guy, C. T., Cardiff, R. D., and Muller, W. J. (1992) *Mol. Cell. Biol.* **12**, 954–961
24. Lin, E. Y., Jones, J. G., Li, P., Zhu, L., Whitney, K. D., Muller, W. J., and

- Pollard, J. W. (2003) *Am. J. Pathol.* **163**, 2113–2126
25. Maglione, J. E., Moghanaki, D., Young, L. J., Manner, C. K., Ellies, L. G., Joseph, S. O., Nicholson, B., Cardiff, R. D., and MacLeod, C. L. (2001) *Cancer Res.* **61**, 8298–8305
26. Zou, J., Dickerson, M. T., Owen, N. K., Landon, L. A., and Deutscher, S. L. (2004) *Mol. Biol. Rep.* **31**, 121–129
27. Lacroix, M. (2008) *Int. J. Cancer* **122**, 1–4
28. Alles, A. J., Warshaw, A. L., Southern, J. F., Compton, C. C., and Lewandrowski, K. B. (1994) *Ann. Surg.* **219**, 131–134
29. Sperti, C., Pasquali, C., Guolo, P., Polverosi, R., Liessi, G., and Pedrazzoli, S. (1996) *Cancer* **78**, 237–243
30. Cuevas, B. D., Winter-Vann, A. M., Johnson, N. L., and Johnson, G. L. (2006) *Oncogene* **25**, 4998–5010
31. Danø, K., Behrendt, N., Hoyer-Hansen, G., Johnsen, M., Lund, L. R., Ploug, M., and Rømer, J. (2005) *Thromb. Haemost.* **93**, 676–681
32. Sabapathy, K. T., Pepper, M. S., Kiefer, F., Möhle-Steinlein, U., Tacchini-Cottier, F., Fetka, I., Breier, G., Risau, W., Carmeliet, P., Montesano, R., and Wagner, E. F. (1997) *J. Cell Biol.* **137**, 953–963
33. Koivunen, E., Saksela, O., Itkonen, O., Osman, S., Huhtala, M. L., and Stenman, U. H. (1991) *Int. J. Cancer* **47**, 592–596
34. Koshikawa, N., Hasegawa, S., Nagashima, Y., Mitsuhashi, K., Tsubota, Y., Miyata, S., Miyagi, Y., Yasumitsu, H., and Miyazaki, K. (1998) *Am. J. Pathol.* **153**, 937–944
35. Miyata, S., Koshikawa, N., Higashi, S., Miyagi, Y., Nagashima, Y., Yanoma, S., Kato, Y., Yasumitsu, H., and Miyazaki, K. (1999) *J. Biochem.* **125**, 1067–1076
36. Paju, A., Vartiainen, J., Haglund, C., Itkonen, O., von Boguslawski, K., Leminen, A., Wahlström, T., and Stenman, U. H. (2004) *Clin. Cancer Res.* **10**, 4761–4768
37. Desmedt, C., Ouriaghli, F. E., Durbecq, V., Soree, A., Colozza, M. A., Azambuja, E., Paesmans, M., Larsimont, D., Buyse, M., Harris, A., Piccart, M., Martiat, P., and Sotiriou, C. (2006) *Int. J. Cancer* **119**, 2539–2545
38. Foekens, J. A., Ries, C., Look, M. P., Gippner-Steppert, C., Klijn, J. G., and Jochum, M. (2003) *Cancer Res.* **63**, 337–341
39. Yamashita, J. I., Ogawa, M., Ikeyi, S., Omachi, H., Yamashita, S. I., Saishoji, T., Nomura, K., and Sato, H. (1994) *Br. J. Cancer* **69**, 72–76
40. Kratz, F., Müller-Driver, R., Hofmann, I., Dreves, J., and Unger, C. (2000) *J. Med. Chem.* **43**, 1253–1256
41. Kratz, F., Warnecke, A., Scheuermann, K., Stockmar, C., Schwab, J., Lazar, P., Drückes, P., Esser, N., Dreves, J., Rognan, D., Bissantz, C., Hinderling, C., Folkers, G., Fichtner, I., and Unger, C. (2002) *J. Med. Chem.* **45**, 5523–5533
42. Jessani, N., Liu, Y., Humphrey, M., and Cravatt, B. F. (2002) *Proc. Natl. Acad. Sci. U.S.A.* **99**, 10335–10340
43. Brown, S., Bernardo, M. M., Li, Z. H., Kotra, L. P., Tanaka, Y., Fridman, R., and Mobashery, S. (2000) *J. Am. Chem. Soc.* **122**, 6799–6800